ELSEVIER

Polymer 44 (2003) 2807–2815

polymer

www.elsevier.com/locate/polymer

Brownian dynamics simulations of the effects of hydrodynamic interactions on the polymer viscoelastic behavior

D.-J. Yang, Y.-H. Lin*

Department of Applied Chemistry, National Chiao Tung University, Hsinchu, Taiwan, ROC

Received 16 August 2002; received in revised form 14 January 2003; accepted 26 January 2003

Abstract

Brownian dynamics simulation is used to investigate the viscoelastic response of the Gaussian chain to a step shear deformation in both the linear and non-linear regions under the influence of hydrodynamic interactions. Both the preaveraged Oseen tensor and the Rotne–Prager tensor are used in the study. In the former case, the simulation results are shown to be in agreement with the expected results calculated using the eigenvalues of the normal modes of motion obtained numerically. It is shown that an initial state with zero second normal-stress difference is generated by the step shear deformation. The subsequent rise of the second normal-stress difference as revealed by the simulation is shown mainly arising from the coupling of the recoil of the stretched bond in the direction of deformation and the anisotropy in the hydrodynamic interaction created by the step deformation.

Keywords: Brownian dynamics simulation; Hydrodynamic interactions; Second normal-stress difference

1. Introduction

As first introduced by Kirkwood and Riseman [1,2] into a polymer system, the pertubation of the solvent flow field caused by the forces experienced by suspending spherical particles leads to a dynamical interaction between beads, the so-called hydrodynamic interaction. At the θ temperature, where the excluded volume effect is absent, the chain dynamic behavior under the influence of hydrodynamic interaction in a dilute solution has been extensively studied theoretically and experimentally. The inclusion of the hydrodynamic interaction into the Langevin equation renders it to become non-linear and unsolvable analytically. Zimm preaveraged the hydrodynamic interaction—the Oseen tensor [3]. Under such an approximation, the diffusion constant and intrinsic viscosity have been calculated and the eigenvalues for the normal modes of motion have also been obtained numerically [3–10]. It has been shown that the large differences between the Rouse theory and the experimental results of the dilute polymer solutions have been basically corrected by the Zimm model [11–14].

In recent years, the Brownian dynamics simulation [15–19] has been used widely to investigate the dynamic and viscoelastic behavior of a polymer chain in a dilute solution, where a detailed theoretical analysis is not possible, such as under the influence of a fluctuating hydrodynamic interaction. In this study, the viscoelastic responses to a step shear strain in the linear and non-linear regions are investigated by the Brownian dynamics simulation. First, in the case of using the preaveraged Oseen tensor, the simulation results are shown to be in agreement with the expected results calculated using the eigenvalues of the normal modes of motion obtained numerically [8]. Then, the non-linear effects revealed from the simulations based on the preaveraged Oseen tensor and the Rotne–Prager tensor [20] are compared. Particularly, the rise of the second normal-stress difference in the latter case is investigated and analyzed.

2. Background

2.1. Basic equations

Consider a Gaussian chain of N beads with positions $\{\mathbf{R}_n\} = (\mathbf{R}_1, \mathbf{R}_2, \ldots, \mathbf{R}_N)$ and connected by springs each

* Corresponding author. Tel.: +886-3573-1631; fax: +886-3572-3764.
E-mail address: yhlin@mail.nctu.edu.tw (Y.-H. Lin).

0032-3861/03/$ - see front matter © 2003 Elsevier Science Ltd. All rights reserved.
doi:10.1016/S0032-3861(03)00152-6

with the mean square bond length $\langle b^2 \rangle$ (denoted simply by b^2 below). In the absence of a macroscopic flow field, the dynamics of the Gaussian chain under the influence of hydrodynamic interaction $\mathbf{H}_{nm}$ with the property $(\partial/\partial\ \mathbf{R}_n)\cdot \mathbf{H}_{nm} = 0$ is described by the Langevin equation [9,10]

$$\frac{\partial \mathbf{R}_n(t)}{\partial t} = -\sum_m \mathbf{H}_{nm}\cdot\frac{\partial U}{\partial \mathbf{R}_m} + \mathbf{g}_n(t) \tag{1}$$

where U is the total spring potential of the chain, $(3kT/b^2)\Sigma_{n=2,\,N}(\mathbf{R}_n - \mathbf{R}_{n-1})^2$, and $\mathbf{g}_n(t)$ arising from the fluctuation force is defined by

$$\langle \mathbf{g}_n(t) \rangle = 0 \tag{2}$$

$$\langle \mathbf{g}_n(t')\mathbf{g}_m(t'') \rangle = 2kT\mathbf{H}_{nm}\delta(t' - t'') \tag{3}$$

For $n = m$, $\mathbf{H}_{nn} = \mathbf{I}/\zeta$, where $\mathbf{I}$ is the unit tensor and ζ is the friction constant experienced by each bead. For a bead with radius a, ζ is given by the Stokes–Einstein equation $\zeta = 6\pi\eta_s a$. For $n \neq m$ two forms of $\mathbf{H}_{nm}$ tensor have been proposed as approximations to the hydrodynamic interaction mediated by the solvent fluid: (a) the Oseen tensor, which treats each bead as a point, is given by:

$$\mathbf{H}_{nm} = \frac{1}{8\pi\eta_s r_{nm}}\left(\frac{\mathbf{r}_{nm}\mathbf{r}_{nm}}{r_{nm}^2} + \mathbf{I}\right) \tag{4}$$

where $\mathbf{r}_{nm} = \mathbf{R}_n - \boldsymbol{R}_m$ and $r_{nm} = |\mathbf{r}_{nm}|$, and (b) the Rotne–Prager tensor given by

$$\mathbf{H}_{nm} = \frac{1}{8\pi\eta_s r_{nm}} \times\left[\left(1 + \frac{2a^2}{3r_{nm}^2}\right)\mathbf{I} + \left(1 - \frac{2a^2}{r_{nm}^2}\right)\frac{\mathbf{r}_{nm}\mathbf{r}_{nm}}{r_{nm}^2}\right] \tag{5}$$

for $r_{nm} \geq 2a$; and

$$\mathbf{H}_{nm} = \frac{1}{6\pi\eta_s a}\left[\left(1 - \frac{9r_{nm}}{32a}\right)\mathbf{I} + \left(\frac{3r_{nm}}{32a}\right)\frac{\mathbf{r}_{nm}\mathbf{r}_{nm}}{r_{nm}^2}\right] \tag{6}$$

for $r_{nm} \leq 2a$. At $r_{nm} = 2a$, Eqs. (5) and (6) are the same. When r_{nm} is very large, the terms containing $(a/r_{nm})^2$ become negligible; and Eq. (5) reduces to Eq. (4).

The preaveraged Oseen tensor for a Gaussian chain is given by

$$\mathbf{H}_{nm} = \frac{\mathbf{I}}{(6\pi^3|n-m|)^{1/2}\eta_s b} \tag{7}$$

2.2. Brownian dynamics simulation

The algorithm for the Brownian dynamics simulation was given by Ermak and McCammon [15]. Denoting $\zeta\mathbf{H}_{nm}$ by $\mathbf{D}^0_{nm}$ and $2(kT/\zeta)\Delta t$ by l^2, Eq. (1) can be transformed into

$$\mathbf{R}_n(s+1) = \mathbf{R}_n(s) - \frac{l^2}{kT}\sum_m \mathbf{D}^0_{nm}\cdot\frac{\partial U}{\partial \mathbf{R}_m} + \Delta\mathbf{r}_n(s) \tag{8}$$

where

$$\langle \Delta\mathbf{r}_n(s) \rangle = 0 \tag{9}$$

$$\langle \Delta\mathbf{r}_n(s')\Delta\mathbf{r}_m(s'') \rangle = \mathbf{D}^0_{nm}l^2\delta_{s',s''} \tag{10}$$

It is understood that the second term on the right side of Eq. (8) is calculated at time-step $s = t_s/\Delta t$. The fluctuations $\{\Delta\mathbf{r}_n(s)\}$ at time-step s can be calculated from the variance–covariance matrix $\mathbf{D}^o_{nm}(s)$ (to express the tensorial property of $\mathbf{D}^o_{nm}(s)$, a $3N \times 3N$ matrix is involved in practice). This can be carried out through the Cholesky decomposition of the $\mathbf{D}^0_{nm}(s)$ matrix and the generation of a random array consisting of $3N$ components with values being either $+1$ or -1, or obtained from a multivariate normal deviate generator such as the RNMVN subroutine listed in the IMSL[1] library. It is well known that the Oseen tensor is not positive definite, when r_{nm} is small. Thus, in the following simulation of chain dynamics, only the preaveraged Oseen tensor and the Rotne–Prager tensor are used.

3. Simulation Results

3.1. A test for the validity of the Brownian dynamics simulation—stress relaxation simulations

The constitutive equation of the Zimm model is given by Ref. [10]

$$\tau(t) = \int_{-\infty}^{t} ckT\sum_{p=1}^{N-1}\frac{1}{S_p}\exp\left(-\frac{(t-t')}{S_p}\right)\boldsymbol{\gamma}_{[0]}(t,t')\mathrm{d}t' \tag{11}$$

where $\boldsymbol{\gamma}_{[0]}(t,t') = \boldsymbol{\delta} - \mathbf{E}(t,t')\cdot\mathbf{E}^T(t,t')$ with $\mathbf{E}(t,t')$ being the deformation gradient tensor between the present time t and a past time t'; c is the number of polymer chains per unit volume; and S_p, the relaxation time of the pth normal mode of motion, is given by

$$S_p = \frac{\zeta b^2}{6kT\lambda_p} \tag{12}$$

with λ_p being the eigenvalue of the modified Rouse matrix [7,8,10].

Using the Stokes–Einstein equation, the hydrodynamic interaction parameter [21] can be written as

$$h^* = \sqrt{\frac{\bar{3}}{\pi}}\ \frac{a}{b} \tag{13}$$

The eigenvalues λ_p of the modified Rouse matrix at different h^* and N values have been calculated numerically for h^* up to 0.3 and N up to 346 [8].

The stress relaxation following a step shear strain λ at $t_s = 0$ for the Zimm model can be obtained from Eq. (11) (in all the discussions and analyses below related to Eq. (11), the number of chains per unit volume, c, and kT will both be

[1] International Mathematical and Statistical Libraries.

set as 1) as

$$\tau_{xy}(t) = \lambda \sum_{p=1}^{N-1} \exp\left(-\frac{t}{S_p}\right) \tag{14}$$

In the Brownian dynamics simulation, a step shear deformation

$$\mathbf{E} = \begin{pmatrix} 1 & \lambda & 0 \\ 0 & 1 & 0 \\ 0 & 0 & 1 \end{pmatrix} \tag{15}$$

is applied to the polymer chain *in an equilibrium state* at time $t_s = 0$, and then the evolution of $\{\mathbf{R}_n(s)\}$ is calculated according to Eq. (8). For the simulation, a large number of identical relaxation processes following a step deformation are repeated and accumulated for averaging. In each repeating cycle, the following quantities at $t_s = s\Delta t$ are calculated

$$S_{xy}(t_s) = -\frac{3}{b^2} \sum_{n=1}^{N-1} x_n(s) y_n(s) \tag{16}$$

$$S_{\alpha\alpha}(t_s) = -\frac{3}{b^2} \sum_{n=1}^{N-1} \alpha_n(s) \alpha_n(s) \qquad (\alpha = x, y, z) \tag{17}$$

where $x_n(s)$, $y_n(s)$ and $z_n(s)$ are the x, y, and z components of the nth bond vector ($\mathbf{r}_n(s) = \mathbf{R}_{n+1}(s) - \mathbf{R}_n(s)$) at time-step s. Then, based on the Kramers form for the stress tensor [10, 22], the shear and normal stresses are obtained from averaging $S_{xy}(t_s)$ and $S_{\alpha\alpha}(t_s)$, respectively, over the repetition, i.e. $\bar{S}_{xy}(t_s)$, and $\bar{S}_{\alpha\alpha}(t_s)$, where the bar over a calculated quantity denotes the (time-)averaging.

Comparison of the results of the Brownian dynamics simulations and those calculated from Eq. (14) using the eigenvalues for polymer chains with $N = 2, 3$, and 10 at $h^* = 0.25$ and different strains has been made. As shown in Fig. 1 for $N = 10$ as an illustration example, the agreement between the two results validate the Brownian dynamics simulation and indicates the potential usefulness of the Brownian dynamics simulation in a case, where an analytical result or a numerically calculated result is not available, such as the case of using the Rotne–Prager tensor for hydrodynamic interaction.

3.2. Effects of the Rotne–Prager tensor

We define the shear modulus $G(t_s)$, the first normal-stress difference function, $\Phi_1(t_s)$ and the second normal-stress difference $M(t_s)$ per spring connector of the chain, respectively, as

$$G(t_s) = -\frac{\overline{S_{xy}}(t_s)}{\lambda(N-1)} \tag{18}$$

$$\Phi_1(t_s) = -\frac{\overline{S_{xx}}(t_s) - \overline{S_{yy}}(t_s)}{\lambda^2(N-1)} \tag{19}$$

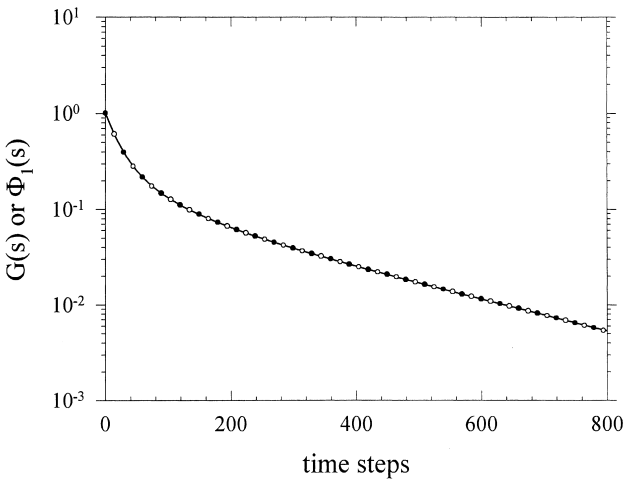

Fig. 1. Comparison of the shear relaxation modulus $G(s)$ (○○○) obtained from the Brownian dynamics simulation ($l = 1$) based on the preaveraged Oseen tensor at $h^* = 0.25$ and $\lambda = 5$ for $N = 10$ with that (solid line) calculated from the Zimm theory using the numerically obtained eigenvalues (the Zimm theoretical curve). Also shown is the observation of the Lodge–Meissner rule, $G(s) = \Phi_1(s)$ (●●●), in the simulation.

and

$$M(t_s) = -\frac{\overline{S_{yy}}(t_s) - \overline{S_{zz}}(t_s)}{(N-1)} \left(\frac{b^2}{3}\right) \tag{20}$$

Besides the agreement in the shear stress relaxation between the Brownian dynamics simulation and calculation based on the eigenvalues as shown in Fig. 1, the following effects expected from the Zimm theory [10] have also been confirmed by the Brownian dynamics simulation:

(1) No non-linear effect in the shear stress relaxation; in other words, the obtained $G(t)$ is independent of strain λ.
(2) The observation of the Lodge–Meissner rule [23], namely, $G(t_s) = \Phi_1(t_s)$, as also shown in Fig. 1.
(3) Zero second normal-stress difference: $M(t_s) = 0$.

When the Rotne–Prager tensor is used for hydrodynamic interaction, the shear stress relaxation curve (denoted by $\bar{S}_{xy}^{RP}(s)$) becomes below that of the Zimm theory (denoted by $\tau_{xy}^{Zimm}(s)$) as shown in Fig. 2 for polymers of $N = 10$ and 21 at $h^* = 0.25$ and $\lambda = 1$. In the long time region, the $\bar{S}_{xy}^{RP}(s)$ and $\tau_{xy}^{Zimm}(s)$ curves parallel each other. This indicates that the use of the Rotne–Prager tensor, instead of the preaveraged Oseen tensor, only affects the fast relaxation modes in the shear stress relaxation curve. Similar results have been obtained by Rey et al. [17].

Furthermore, in the case of using the Rotne–Prager tensor, as shown in Fig. 3, the non-linear effect in the shear stress relaxation up to the strain $\lambda = 5$ is weak, but indeed observable. However, as shown in Fig. 4, the Lodge–Meissner rule remains observed in the simulation based on the Rotne–Prager tensor. The most prominent effect arising from using the Rotne–Prager tensor is the non-zero second

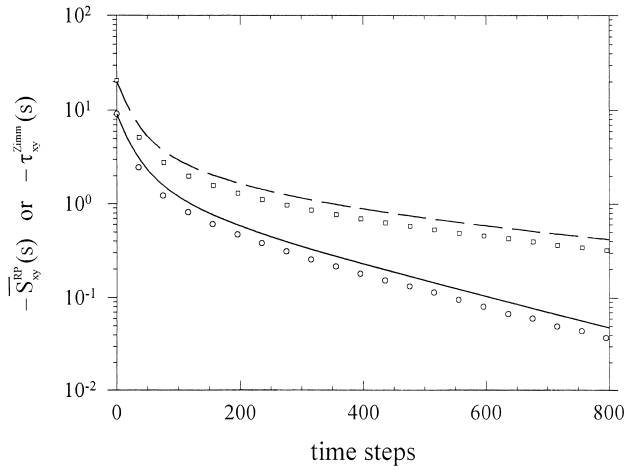

Fig. 2. Comparison of the shear stress relaxation curves, $-\bar{S}_{xy}^{RP}(s)$, obtained from the simulation ($l = 1$) based on the Rotne–Prager tensor at $h^* = 0.25$ and $\lambda = 1$ for $N = 10$ (○○○) and $N = 21$ (□□□) with the Zimm theoretical curves, $-\tau_{xy}^{Zimm}(s)$ (solid line for $N = 10$; and dashed line for 21).

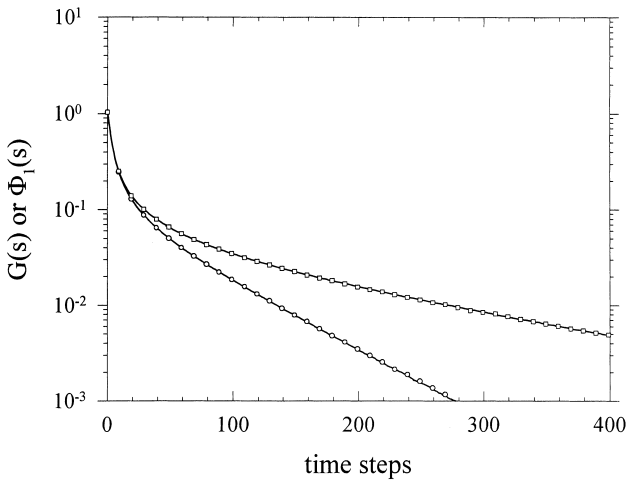

Fig. 4. The Lodge–Meissner rule as observed in the simulation ($l = 2$) based on the Rotne–Prager tensor at $h^* = 0.25$ and $\lambda = 5$ for $N = 10$ (○○○ for $G(s)$ and lower solid line for $\Phi_1(s)$) and $N = 21$ (□□□ for $G(s)$ and upper solid line for $\Phi_1(s)$).

normal-stress difference. Shown in Fig. 5 are the $M(t_s)$ curves obtained at $h^* = 0.25$ and $\lambda = 5$ for $N = 2, 3, 10$, and 21, which are quite different from those for $G(t_s)$ and $\Phi_1(t_s)$ in shape. It can be noticed that there is a rising phase and a declining phase in $M(t_s)$. This strongly suggests that the constitutive equation for a system with the Rotne–Prager tensor for hydrodynamic interaction would be quite different from the form of the Zimm model (Eq. (11)).

Right after the step shear deformation, Eq. (15), is applied at $t_s = 0$, $M(0) = 0$, because the deformation does not create a difference in the configuration distribution of the bond vectors between y and z directions, i.e. $\overline{y(0)y(0)} = \overline{z(0)z(0)}$ for any bond vector. In fact, if the affine deformation is assumed as in the present study and in most cases, the stress tensor $\boldsymbol{\tau}(0)$ right after the application of a step strain is the same for a Gaussian chain regardless of whether there is a hydrodynamic interaction between the beads or what its form is. As the time goes on ($t_s > 0$), the velocity field at a certain part of the chain induced by the force at another part of the chain will change each other's configuration distribution. Then, the question is whether there is a transfer of configuration change from one direction to another direction. In the case of the Zimm model, where the hydrodynamic interaction is preaveraged and remains the same and isotropic for any pair of beads regardless of the deformation, such a transfer cannot occur. Thus, in the Zimm theory, $M(t_s)$ remains zero for $t_s > 0$. This is clearly not the case, when the Rotne–Prager tensor is used for the hydrodynamic interaction.

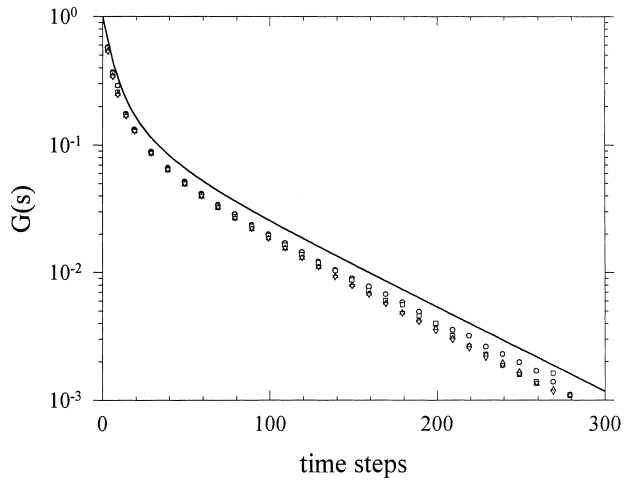

Fig. 3. The strain dependence of the shear relaxation modulus $G(s)$ (○ for $\lambda = 0.5$; □ for $\lambda = 1$; Δ for $\lambda = 3$; and ∇ for $\lambda = 5$) as observed from the simulation ($l = 2$) based on the Rotne–Prager tensor at $h^* = 0.25$ for $N = 10$. Also shown is the Zimm theoretical curve (solid line).

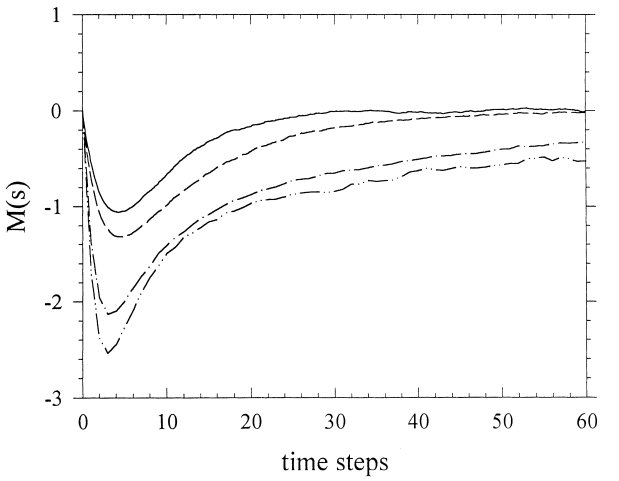

Fig. 5. The second normal-stress difference, $M(s)$ (Eq. (20)), as observed in simulations ($l = 2$) based on the Rotne–Prager tensor at $h^* = 0.25$ and $\lambda = 5$ for $N = 2$ (—), 3 (- - -), 10 (-·-·-), and 21 (-···-).

3.3. Analysis of the rise of the second normal-stress difference

As shown in Fig. 5, the $M(s)$ peak position depends on N only weakly and occurs in the short time region. This phenomenon suggests that the basic mechanism for the rise of the second normal-stress difference should be quite the same for a short chain as for a long chain—basically a local phenomenon. For simplifying the analysis, we first consider the elastic-dumbbell case. For $N = 2$, Eq. (8) can be expressed as

$$\mathbf{r}(s+1) = Z\mathbf{r}(s) + \mathbf{w}(s) + \mathbf{v}(s) \tag{21}$$

where $\mathbf{r}(s)(= \mathbf{R}_2(s) - \mathbf{R}_1(s))$ is the bond vector at time-step s,

$$Z = 1 - 2S = 1 - \frac{3l^2}{b^2} \tag{22}$$

$$\mathbf{w}(s) = 2S\mathbf{D}^0_{21}(s)\cdot\mathbf{r}(s) \tag{23}$$

and

$$\mathbf{v}(s) = \Delta\mathbf{r}_2(s) - \Delta\mathbf{r}_1(s) \tag{24}$$

According to Eqs. (17) and (20), we can calculate $M(s)$ from the yy and zz components of $\overline{\mathbf{r}(s)\cdot\mathbf{r}(s)}$. Thus, from Eq. (21), we can obtain

$$M(s+1) = Z^2M(s) + \sum_{i=1}^{5}\Delta M_i(s) \tag{25}$$

where $\{\Delta M_i(s)\}$ can be obtained from taking the differences between the yy and zz components of the following dot products

$$\overline{\mathbf{w}(s)\cdot\mathbf{w}(s)} \rightarrow \Delta M_1(s) \tag{26}$$

$$\overline{\mathbf{v}(s)\cdot\mathbf{v}(s)} \rightarrow \Delta M_2(s) \tag{27}$$

$$2Z\overline{\mathbf{r}(s)\cdot\mathbf{w}(s)} \rightarrow \Delta M_3(s) \tag{28}$$

$$2Z\overline{\mathbf{r}(s)\cdot\mathbf{v}(s)} \rightarrow \Delta M_4(s) \tag{29}$$

$$2\overline{\mathbf{w}(s)\cdot\mathbf{v}(s)} \rightarrow \Delta M_5(s) \tag{30}$$

Since $M(0) = 0$ for any strain λ, Eq. (25) can be rewritten as

$$M(s) = \sum_{i=1}^{5} M_i(s) \tag{31}$$

with

$$M_i(s+1) = Z^2M_i(s) + \Delta M_i(s) \tag{32}$$

and the initial conditions

$$M_i(0) = 0 \qquad \text{for all } i \tag{33}$$

Using Eqs. (32) and (33), each component of $M(s), M_i(s)$, can be calculated from $\Delta M_i(s)$ obtained using Eqs. (26)–(30) in the simulation.

$M_4(s)$ and $M_5(s)$ show up as noises around zero, as one would expect from Eqs. (29) and (30). $M_1(s)$, $M_2(s)$, and $M_3(s)$ are non-zero with $|M_3(s)| > |M_2(s)| \gg |M_1(s)|$. The contribution of $M_1(s)$ to the total, $M(s)$, is negligible. As shown in Fig. 6, $M_2(s)$ and $M_3(s)$ have opposite signs; and the total second normal-stress difference $M(s)$ results mainly from their partial mutual cancellation.

Using Eq. (23), ΔM_3 (Eq. (28)) can be expressed by

$$\Delta M_3 = A^3_{yy} - A^3_{zz} \tag{34}$$

where (Note: The superscript of A does not represent an exponent, but is an index as in the rest of the paper.)

$$A^3_{yy} = 4SZ\overline{(\mathbf{r}(s)\cdot\mathbf{D}^0_{12}(s)\cdot\mathbf{r}(s))_{yy}} \tag{35}$$

and, A^3_{zz} and A^3_{xx} have a corresponding definition.

At the same time, using Eqs. (10) and (24), $\Delta M_2(s)$ (Eq. (27)) can be obtained as

$$\Delta M_2 = A^2_{yy} - A^2_{zz} \tag{36}$$

where

$$\begin{aligned} A^2_{yy} &= \overline{(\Delta\mathbf{r}_2\cdot\Delta\mathbf{r}_2)_{yy}} + \overline{(\Delta\mathbf{r}_1\cdot\Delta\mathbf{r}_1)_{yy}} - 2\overline{(\Delta\mathbf{r}_2\cdot\Delta\mathbf{r}_1)_{yy}} \\ &= 2l^2[1 - \overline{(\mathbf{D}^0_{12})_{yy}}] \end{aligned} \tag{37}$$

and, A^2_{zz} and A^2_{xx} have a corresponding definition.

Here, we shall do an analytical calculation on the $A^3_{\alpha\alpha}$ and $A^2_{\alpha\alpha}$ values created right after the application of the step shear deformation. Assuming that the probability is small for the distance between the two beads to be short and comparable to the bead radius, a, we shall use the Oseen tensor to approximate the Rotne–Prager tensor in the calculation. Denote by $x_0 + \lambda y_0, y_0$, and z_0 the x, y, and z components of $\mathbf{r}$ right after the application of the step shear deformation (Eq. (15)). Then A^3_{yy} right after the step deformation can be obtained from Eq. (35) by changing the time averaging with the assembly averaging, which is

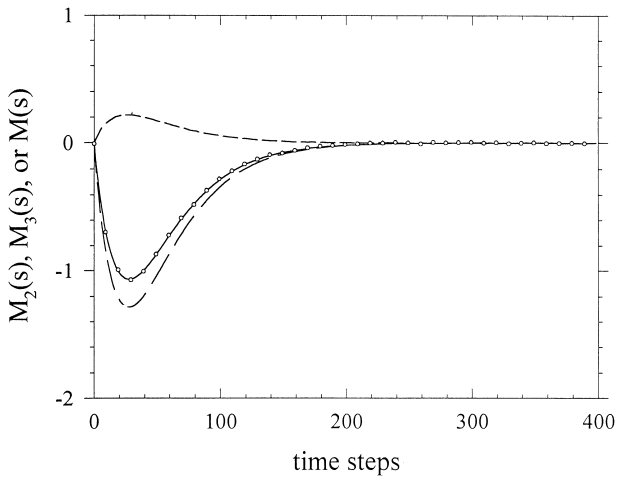

Fig. 6. The $M_2(s)$ (- - -) and $M_3(s)$ (– –) curves calculated through Eq. (32) from $\Delta M_2(s)$ and $\Delta M_3(s)$ which are obtained, using Eqs. (27) and (28), respectively, from the simulation ($l = 0.8$) based on the Rotne–Prager tensor at $h^* = 0.25$ and $\lambda = 5$ for $N = 2$. Also shown is the comparison of the sum (—) of $M_2(s)$ and $M_3(s)$ with that (○) obtained directly from averaging the yy and zz components of $\mathbf{r}(s)\cdot\mathbf{r}(s)$ in the simulation.

then approximated by the averaging over all orientations

$$A^3_{yy} = K\left[\left\langle \frac{(x_0+\lambda y_0)^2 y_0^2 + y_0^4 + y_0^2 z_0^2}{R^{3/2}} \right\rangle + \left\langle \frac{y_0^2}{R^{1/2}} \right\rangle\right]$$
$$\approx K\langle|\mathbf{r}|\rangle_{\mathrm{eq}}\left[\left\langle \frac{V^2u_y^2 + u_y^4 + u_y^2u_z^2}{U^{3/2}} \right\rangle_{\mathbf{u}} + \left\langle \frac{u_y^2}{U^{1/2}} \right\rangle_{\mathbf{u}}\right] \quad (38)$$

where $K = 3aSZ$; u_α ($\alpha = x, y$, and z) is the α component of the unit vector $\mathbf{u}$ representing the orientation of the dumbbell in the equilibrium state; $R(\lambda) = (x_0+\lambda y_0)^2 + y_0^2 + z_0^2$; $V(\lambda) = u_x + \lambda u_y$; $U(\lambda) = 1 + 2\lambda u_x u_y + \lambda^2 u_y^2$; and $< >_{\mathbf{u}}$ denotes averaging over all orientations of $\mathbf{u}$, while $< >_{\mathrm{eq}}$ denotes equilibrium-state averaging. The expressions for A^3_{zz} and A^3_{xx} can be similarly obtained. By the same procedure as used in obtaining Eq. (38), A^2_{yy} is obtained from Eq. (37) as

$$A^2_{yy} \approx 2l^2\left[1 - \frac{3a}{4}\left\langle \frac{1}{|\mathbf{r}|} \right\rangle_{\mathrm{eq}} \left\langle \frac{u_y^2}{U^{3/2}} + \frac{1}{U^{1/2}} \right\rangle_{\mathbf{u}}\right] \quad (39)$$

The expressions for A^2_{zz} and A^2_{xx} can be similarly obtained. For an elastic dumbbell with $\langle\mathbf{r}^2\rangle = 100$ as used in this study, it has been shown by the Monte Carlo simulation that $\langle|\mathbf{r}|\rangle_{\mathrm{eq}} = 9.23$ and $\langle 1/|\mathbf{r}|\rangle_{\mathrm{eq}} = 0.138$ [24]. Using these values, $A^3_{\alpha\alpha}$ and $A^2_{\alpha\alpha}$ ($\alpha = x, y$, and z) calculated at $\lambda = 3$ and 5 are in close agreement with the simulation results as shown in Table 1.

From comparing the expressions for A^3_{yy} and A^3_{zz}, we see that the main cause for the second normal-stress difference is the particular conformational anisotropy of the polymer chain after the step shear deformation for giving $A^3_{yy} < A^3_{zz}$. As indicated by Eqs. (36) and (37), ΔM_2 arises from the difference between the yy and zz components of $\mathbf{D}^0_{12}$ which is created by the step shear deformation. A^2_{yy} is larger than A^2_{zz} basically for a similar reason as explained above. Driven by fluctuations (Eqs. (24) and (27)), M_2 having an opposite sign to that of M_3 cancels out part of the second normal-stress difference due to M_3.

The above calculations for $\{A^3_{\alpha\alpha}\}$ and $\{A^2_{\alpha\alpha}\}$ (Table 1) are only possible for right after the application of the step shear deformation. After the chain configuration 'passing' through the Langevin equation (Eq. (21)), the simulation results of $\{A^3_{\alpha\alpha}(s)\}$ and $\{A^2_{\alpha\alpha}(s)\}$ are shown in Figs. 7 and 8.

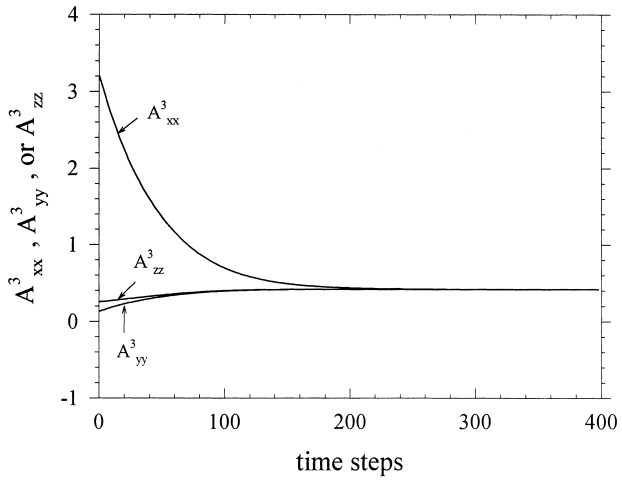

Fig. 7. The time dependence of A^3_{xx}, A^3_{yy}, and A^3_{zz} (see Eq. (35)) obtained from the simulation ($l = 0.8$) based on the Rotne–Prager tensor at $h^* = 0.25$ and $\lambda = 5$ for $N = 2$.

As the system returns to the equilibrium state at large s, $A^3_{xx} = A^3_{yy} = A^3_{zz}$, and $A^2_{xx} = A^2_{yy} = A^2_{zz}$. We can consider $A^3_{xx}(s)$ and $A^2_{xx}(s)$ as contributions over a time step to the change of $\overline{xx}$ from the two 'sources' as described by Eqs. (28) and (27), respectively (the same explanation for the yy and zz components here and below). These contributions counter the decrease of $\overline{xx}$ due to the mechanism corresponding to the first term of Eq. (25), namely,

$$Z^2\overline{x(s)x(s)} \rightarrow \overline{x(s+1)x(s+1)} \quad (40)$$

with $Z < 1$ (Eq. (22)). Thus, at large s, the three components of ΔM_3 (i.e. $\{A^3_{\alpha\alpha}\}$) and of ΔM_2 (i.e. $\{A^2_{\alpha\alpha}\}$) (also of ΔM_1, which has been neglected in the analysis and discussion here, because of its small magnitude) reach some, identical, *positive* steady-state values, respectively, which counteract the decreasing effect due to Eq. (40) so as to maintain the equilibrium bond length and the equipartition principle. It is mainly the differences between A^3_{yy} and A^3_{zz}, and between A^2_{yy} and A^2_{zz} in the off-equilibrium state caused by the step shear deformation that are responsible for the occurrence of the second normal-stress difference. Eventually all the anisotropy in the system has to relax to zero. The combination of the build-up in the early stage by the mechanism described above and the eventual total

Table 1
Comparison of the initial values of A^3_{xx}, A^3_{yy}, A^3_{zz} and of A^2_{xx}, A^2_{yy}, A^2_{zz}, which have been obtained from the calculations based on the averaging over all orientations and from the simulations, at the applied step shear strains: $\lambda = 3$ and 5. Both the calculation and simulation results are obtained with $l = 0.8$

	$\lambda = 3$		$\lambda = 5$	
	From calculation	From simulation	From calculation	From simulation
A^3_{xx}	1.897	1.866	3.236	3.209
A^3_{yy}	0.2098	0.2029	0.1325	0.1300
A^3_{zz}	0.3320	0.3156	0.2656	0.2540
A^2_{xx}	0.9028	0.9331	0.9719	0.9985
A^2_{yy}	1.005	1.016	1.078	1.085
A^2_{zz}	0.9650	0.9908	1.040	1.062

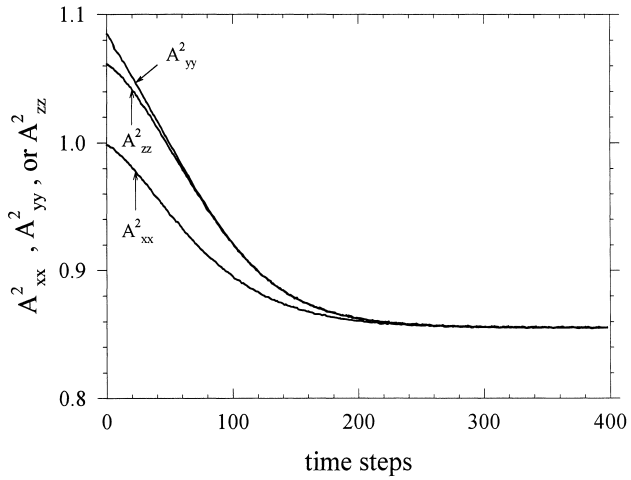

Fig. 8. The time dependence of A^2_{xx}, A^2_{yy}, and A^2_{zz} (see Eq. (37)) obtained from the simulation ($l = 0.8$) based on the Rotne–Prager tensor at $h^* = 0.25$ and $\lambda = 5$ for $N = 2$.

relaxation gives rise to the peak in the second normal-stress difference, where the build-up rate equals the relaxation rate.

We can also explain the rise of the second normal-stress difference in another physical way. From the above discussion, we know that the **w** term in Eq. (21), which is expressed by Eq. (23), is the main factor that gives rise to the second normal-stress difference. Right after the step shear deformation, a large driving force that greatly affects the chain conformation in the early stage of shear stress relaxation is the recoil of the x component of the stretched bond, namely, a large decrease from the initial value $x_0 + \lambda y_0$. A coupling of this driving force with the anisotropic part of the hydrodynamic interaction will lead to a shortening of the projections of the bond in y and z directions. According to Eqs. (21) and (23), it depends on the magnitudes of $(\mathbf{D}^0_{12})_{yx}$ and $(\mathbf{D}^o_{12})_{zx}$ how effectively a shortening of the projection of the bond in the x direction (say, $-\Delta x$) will lead to a decrease in y and z (say, $-\Delta y$ and $-\Delta z$). We can estimate the relative magnitude of these two components by calculating their averages similar to what is done in Eq. (38). In general $\langle(\mathbf{D}^0_{12})_{yx}\rangle \gg \langle(\mathbf{D}^0_{12})_{zx}\rangle$. For instance, at $h^* = 0.25$, $\lambda = 5$, $\langle(\mathbf{D}^0_{12})_{yx}\rangle \approx 1.7 \times 10^{-3}$ while $\langle(\boldsymbol{D}^o_{12})_{zx}\rangle < 10^{-11}$. Thus, a shortening in x leads to a larger shortening in y. As a result, $\overline{y(s)y(s)} < \overline{z(s)z(s)}$ or $M(s) < 0$, giving rise to the second normal-stress difference.

In the above analysis, we have considered the $N = 2$ case, where there is no coupling between different bonds, which one needs to consider for $N > 2$. In view of the peak position of $M(s)$ being a weak function of N as shown in Fig. 5, the coupling terms may play only minor roles which modify the main mechanism as described above for the $N = 2$ case. The number of terms that need to be considered increases greatly with increasing N. In the following, we study the case of $N = 3$ to show the modification effects due to some important cross terms. Denoting the two bonds in the $N = 3$ case as $\mathbf{r}_1(= \mathbf{R}_2 - \mathbf{R}_1)$ and $\mathbf{r}_2(= \mathbf{R}_3 - \mathbf{R}_2)$, we obtain from Eq. (8)

$$\mathbf{r}_1(s+1) = Z\mathbf{r}_1(s) + \mathbf{w}_1(s) + \mathbf{v}_1(s) + S\mathbf{r}_2(s) - \mathbf{u}_2(s) \quad (41)$$

where

$$\mathbf{w}_1(s) = 2S\mathbf{D}^0_{21}(s)\cdot\mathbf{r}_1(s) \quad (42)$$

$$\mathbf{v}_1(s) = \Delta\mathbf{r}_2(s) - \Delta\mathbf{r}_1(s) \quad (43)$$

$$\mathbf{u}_2(s) = S(\mathbf{D}^0_{12}(s) + \mathbf{D}^0_{23}(s) - \mathbf{D}^0_{13}(s))\cdot\mathbf{r}_2(s) \quad (44)$$

An equation equivalent to Eq. (41) can in the same way be obtained for the calculation of $\mathbf{r}_2(s+1)$. The normal stress differences for an $N = 3$ chain can be obtained from the time-averaging calculation of the components of $\mathbf{r}_1(s)\cdot\mathbf{r}_1(s) + \mathbf{r}_2(s)\cdot\mathbf{r}_2(s)$. Statistically, bond one and bond two are equivalent. Thus, we need to consider only one of them (bond one is chosen here). Similar to Eq. (31), we have

$$M(s) = \sum_{i=1}^{14} M_i(s) \quad (45)$$

with Eqs. (32) and (33) equally applicable for $i = 1$ to 14.

In substituting the various $\Delta M_i(s)$ terms into Eq. (32), we need to consider only the ΔM_2, ΔM_3, ΔM_7, and ΔM_8 terms which can be obtained by taking the differences between the yy and zz components of the following dot products; the other terms give rise to either noises around zero or negligible contributions to $M(s)$:

$$\overline{\mathbf{v}_1(s)\cdot\mathbf{v}_1(s)} \to \Delta M_2(s) \quad (46)$$

$$2Z\overline{\mathbf{r}_1(s)\cdot\mathbf{w}_1(s)} \to \Delta M_3(s) \quad (47)$$

$$2ZS\overline{\mathbf{r}_1(s)\cdot\mathbf{r}_2(s)} \to \Delta M_7(s) \quad (48)$$

$$2Z\overline{\mathbf{r}_1(s)\cdot\mathbf{u}_2(s)} \to \Delta M_8(s) \quad (49)$$

$\Delta M_2(s)$ and $\Delta M_3(s)$ given by Eqs. (46) and (47) are equivalent to those given by Eqs. (27) and (28), respectively, for the $N = 2$ case; however, $\Delta M_7(s)$ and $\Delta M_8(s)$ are due to couplings between bond 1 and bond 2. The obtained $M_2(s)$, $M_3(s)$, $M_7(s)$, and $M_8(s)$ curves are shown in Fig. 9. As also shown in the figure, the sum of these four curves are in close agreement with the $M(s)$ curve which has been calculated directly from averaging the yy and zz components of $\mathbf{r}_1(s)\cdot\mathbf{r}_1(s)$, confirming that the other terms can be neglected. $M_2(s)$ and $M_3(s)$ are similar to their counterparts in Fig. 6. The small differences should be due to the small dynamic difference of a single bond motion between the $N = 2$ and $N = 3$ cases. It has been shown in the free-draining case that the time-auto-correlation function of a single bond depend on N only weakly, particularly in the short-time region [24]; it is expected to be similar here. The coupling contributions, $M_7(s)$ and $M_8(s)$, are much smaller than $M_3(s)$ in magnitude, and as revealed in Fig. 9 cancel out each other to some extent. The $M(s)$ peak occurring in the short-time region is enhanced by the contributions of $M_7(s)$ and $M_8(s)$, and is higher than that of the $N = 2$ case. The phenomenon as shown in Fig. 5 that the $M(s)$ peak becomes greater with increasing N should be due to the

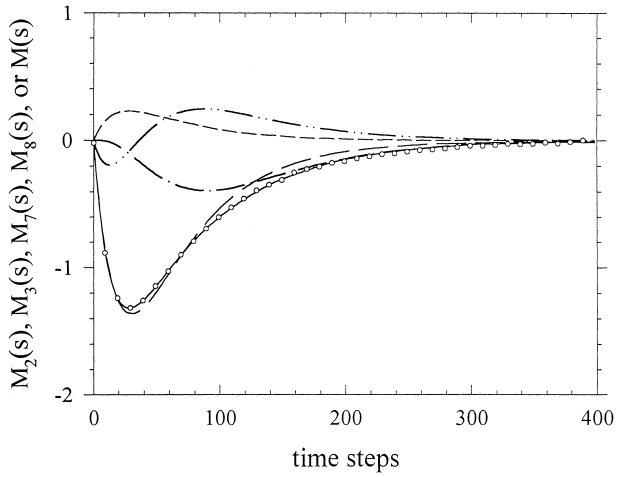

Fig. 9. The $M_2(s)$ (- - -), $M_3(s)$ (– –), $M_7(s)$ (-·-·-), and $M_8(s)$ (-···-) curves obtained, through the use of Eqs. (46)–(49), respectively, from the simulation ($l = 0.8$) based on the Rotne–Prager tensor at $h^* = 0.25$ and $\lambda = 5$ for $N = 3$. Also shown is the comparison of the sum (—) of $M_2(s)$, $M_3(s)$, $M_7(s)$, and $M_8(s)$ with that (○) obtained directly from averaging $\mathbf{r}_1(s)\cdot\mathbf{r}_1(s)$ in the simulation.

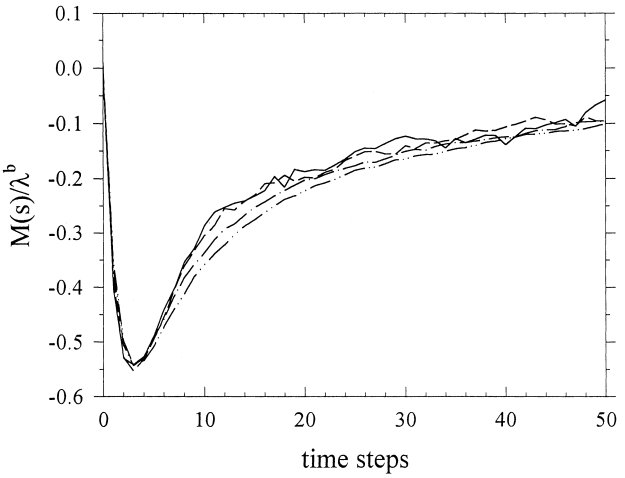

Fig. 10. The $M(s)/\lambda^b$ curves at different λ values (— at $\lambda = 0.5$; - - - at $\lambda = 1$; -·-·- at $\lambda = 3$; and -···- at $\lambda = 5$) for $N = 10$. b is first found to be 1.8 by matching the peaks of the curves at $\lambda = 0.5$ and 1. By matching the other curves to the thus obtained two curves at the peak, b is found to be 1.1 at $\lambda = 3$ and 0.85 at $\lambda = 5$.

coupling terms in a way similar to what occurs in the $N = 3$ case. As revealed for the $N = 3$ case, however, the peak position of $M(s)$ in time should still be greatly influenced by the peak of $M_3(s)$ because of its relatively large magnitude. Because the $M_3(s)$ peak is a very weak function of N, this explains why the observed $M(s)$ peak position depends on N weakly. As shown in Fig. 9, the coupling terms contribute to the long-time region of $M(s)$ as well as to the peak height of $M(s)$.

4. Discussion

The second normal-stress difference has a complicated strain dependence, as indicated by Eq. (38) and (39) for A^3_{yy} and A^2_{yy}, respectively. In Fig. 10, we show the second normal-stress difference at different strains with the peak height matched for a chain with $N = 10$. In doing so, the second normal-stress difference is divided by a factor λ^b, where b is an adjustable parameter. These 'normalized' curves basically have the same shape. The strain dependence of b indicates the complicated strain dependence of the second normal-stress difference.

From this simulation study it is found that the second normal-stress difference while having the opposite sign is much smaller than the first normal-stress difference in magnitude (for instance about 5% at $\lambda = 1$ in the long time region). In steady shear flow, the first and second normal-stress coefficients Ψ_1 and Ψ_2 (as defined in Ref. [10]) of the Hookean dumbbell with unaveraged Oseen tensor have been studied numerically by Fan [25] giving Ψ_2 to be negative and $|\Psi_2|/|\Psi_1|$ to have a magnitude comparable to the experimental results [26]. The Brownian dynamics simulation of Diaz et al. [27] (using the Oseen tensor, with a modified form when $r < 2a$ [28]) appeared to support the viscosity and Ψ_1 obtained by Fan as a function of shear rate but due to the statistical error could not produce a detectable departure of Ψ_2 from 0.

5. Summary

The viscoelastic properties of a dilute polymer solution system in the θ condition is studied by assuming a mean-field friction constant. The viscoelastic response of the system to a step shear deformation can be studied by the Brownian dynamics simulation on a single polymer chain. When the preaveraged Oseen tensor, which is isotropic and does not change with deformation, is used in the Brownian dynamics simulation, the viscoelastic results of the Zimm model, whose eigenvalues of the normal modes can be obtained numerically, are quantitatively reproduced. This shows that the Brownian dynamics simulation can replace the numerical solution in showing the result of a particular model. This also indicates that the Brownian dynamics simulation becomes even more valuable, when a numerical solution is impossible to obtain, such as in the case where a fluctuating hydrodynamic interaction is involved.

As shown in this study, the most outstanding phenomenon that occurs when the Rotne–Prager tensor is used for the hydrodynamic interaction in the simulation is the non-zero second normal-stress difference, which has an opposite sign to the first normal-stress difference. The detailed mechanism for the rise of the second normal-stress difference in the $N = 2$ case has been analyzed. It is shown that when the ensemble averaging is approximated by the averaging over all orientations, the initial values of A^2_{xx}, A^2_{yy}, and A^2_{zz}; and A^3_{xx}, A^3_{yy}, and A^3_{zz} following the application of a step shear strain can be calculated. The

calculated values with the Rotne–Prager tensor approximated by the Oseen tensor are in close agreement with the results obtained from the simulation. Such an agreement supports the picture that the anisotropy in hydrodynamic interaction caused by the applied step strain gives rise to the second normal-stress difference. In the studies of the steady-state shear flow case, it has also been generally concluded that the second normal-stress difference arises from the anisotropy in hydrodynamic interaction [25,27–29]. However, in this study we show that there are different routes for the anisotropy in hydrodynamic interaction to give a non-zero value to the second normal-stress difference and that the M_3 term, which reflects the kind of interaction as given by Eqs. (34) and (35), is the most important contribution. The mechanism of the $\Delta M_3(s)$ interaction in causing the rise of the second normal-stress difference may be pictured as the coupling of the recoil of the stretched bond in the direction of deformation and the anisotropy in hydrodynamic interaction created by the step shear deformation.

The $N = 3$ case is studied for the effects of the coupling terms between different bonds. While the coupling terms cannot be neglected, the terms confined to a single bond have the largest effect, in particular, the $M_3(s)$ term, which is weakly dependent on N. Because of the dominance of the $M_3(s)$ term, the peak position of the second normal-stress difference occurs in the short time region and is a weak function of N. However, the contributions of the coupling terms make the peak height of the second normal-stress difference per bond increases with increasing N.

When a fluctuating hydrodynamic interaction is involved, a numerical solution is in general very difficult to obtain. Mainly because of experimental difficulties, the second normal-stress difference has rarely been measured. In such a situation of lacking both numerical and experimental results, the Brownian dynamics simulation becomes particularly valuable. In this study, the mechanism for the rise of the second normal-stress difference has been analyzed in detail.

Acknowledgements

This work is supported by the National Science Council (NSC 89-2113-M-009-011 & -030), and the simulation is carried out at the National Center for the High-Performance Computing.

References

[1] Kirkwood JG, Riseman J. J Chem Phys 1948;16:565.
[2] Kirkwood JG. J Polym Sci 1954;12:1.
[3] Zimm BH. J Chem Phys 1956;24:269.
[4] Zimm BH, Roe GM, Epstein LF. J Chem Phys 1956;24:279.
[5] Osaki K. Macromolecules 1972;5:141.
[6] Yamakawa H. Modern Theory of Polymer Solutions. New York: Harper & Row; 1971.
[7] Lodge AS, Wu YJ. Rheol Acta 1971;10:539.
[8] Sammler RL, Schrag JL, Lodge AS. Exact Eigenvalue Spectra for Calculation of Dynamic Functions for Dilute Polymer Solutions Based on the Bead-Spring Model, University of Wisconsin Rheology Research Center Report No. 82; June 1982.
[9] Doi M, Edwards SF. The Theory of Polymer Dynamics. Oxford University Press: New York; 1986.
[10] Bird RB, Curtiss CF, Armstrong RC, Hassager O, 2nd ed. Dynamics of Polymeric Liquids: Kinetic Theory, vol. 2. New York: Wiley; 1987.
[11] Han CC, Crackin FL. Polymer 1979;20:427.
[12] Nose T, Chu B. Macromolecules 1979;12:590.
[13] Schmidt M, Burchard W. Macromolecules 1981;14:210.
[14] Adachi K, Kotaka T. Macromolecules 1987;20:2018.
[15] Ermak DL, McCammon JA. J Chem Phys 1978;69:1352.
[16] Fixman M. Macromolecules 1981;14:1710.
[17] Rey A, Freire JJ, Garcia de la Torre J. J Chem Phys 1990;92:6278.
[18] Rey A, Freire JJ. J Chem Phys 1995;102:6900.
[19] Kroger M, Alba-Perez A, Laso M, Ottinger HC. J Chem Phys 2000; 113:4767.
[20] Rotne J, Prager S. J Chem Phys 1969;50:4831. Yamakawa H. J Chem Phys 1970;53:436.
[21] Thurston GB, Peterlin A. J Chem Phys 1967;46:4881.
[22] Kramers HA. Physica 1944;11:1. and Ref. [10].
[23] Lodge AS, Meissner J. Rheol Acta 1972;11:351.
[24] Lin YH, Luo ZH. J Chem Phys 2000;112:7219.
[25] Fan XJ. J Chem Phys 1986;85:6237.
[26] Christiansen EB, Leppard WR. Trans Soc Theol 1974;18:65.
[27] Diaz FG, Garcia de la Torre J, Freire JJ. Polymer 1989;30:259.
[28] Diaz FG, Iniesta A, Garcia de la Torre J. J Chem Phys 1987;87:6021.
[29] Shafer RH. Macromolecules 1976;9:895.